Available online at www.sciencedirect.com
ScienceDirect
Journal of Nuclear Materials 363–365 (2007) 1403–1408
journal of nuclear materials
www.elsevier.com/locate/jnucmat

Effect of recombination and ionization on the analysis of Mach and single probes in un-magnetized and magnetized plasmas of MAP-II and DiPS devices

K.-S. Chung [a,b,*], S. Kado [a], H.-J. Woo [b], Y.-J. Seo [b], T. Shikama [c], F. Scotti [c], G.-S. Choi [b], T. Lho [d]

[a] *High Temperature Plasma Ctr., The University of Tokyo, Kashiwa, Chiba, Japan*
[b] *Department of Electrical Engineering, Hanyang University, Seoul 133-791, Republic of Korea*
[c] *Graduate School of Engineering, The University of Tokyo, Bunkyo, Tokyo, Japan*
[d] *Division of Plasma Application, National Fusion Research Ctr., Daejeon, Republic of Korea*

Abstract

For the analysis of atomic processes such as recombination and ionization in the divertor plasmas, we have developed a fast-scanning multiple probe system, which is composed of single, Mach and emissive probes along with Thomson scattering system at the material and plasma (MAP)-II divertor simulator with low magnetic field (about 200 G). Measured spatial variations of electron density, electron temperature, flow velocity and plasma potential will be given in comparison with those by Thomson scattering method. To analyze the data, a new fluid model on the ion collection to a probing object in un-magnetized plasmas is developed including electron–ion recombination, molecular activated recombination and ionization. This system is applied to another divertor simulator, divertor plasma simulator (DiPS), with higher magnetic field (up to 2 kG).

PACS: 52.70.−m; 52.70.Nc; 52.30.−q; 52.40.Hf

Keywords: Plasma flow; Probes; Recombination; Divertor plasma

1. Introduction

Edge conditions are important in influencing the characteristics of tokamak plasmas, and many problems such as detached plasmas, flow reversal and the strong heat flux limit are linked to the transport of momentum in the scrape-off layer. Although significant ion drift resulting from scrape-off flow plays an important role in impurity transport and fluctuation levels, it is difficult to accurately measure the flows [1]. Recombination processes in the fusion edge plasmas to achieve a detached plasma becomes a very promising scenario for the reduction of particle and heat fluxes onto the divertor targets. In addition to electron–ion recombination processes

* Corresponding author. Address: Department of Electrical Engineering, Hanyang University, Seoul 133-791, Republic of Korea.
E-mail address: kschung@hanyang.ac.kr (K.-S. Chung).

0022-3115/$ - see front matter © 2007 Published by Elsevier B.V.
doi:10.1016/j.jnucmat.2007.01.264

characterized by radiative and three-body recombinations, molecular assisted/activated recombination processes induced by the hydrogen [2] or hydrocarbon [3] puffing recently have shown the capability of contributing to the volume recombination. The conditions for each process to be effective strongly depend on electron temperature and electron density. Although basic plasma physics experiments in linear machines such as material and plasma (MAP)-II [4], divertor plasma simulator (DiPS) [5], and other devices in the references therein, aimed at analyzing the magnetized presheath region of simulated tokamak edge plasmas, and have shifted toward the test of materials relevant to large fusion devices, they can still perform physics experiment related dust, radiation cooling and other atomic processes.

The goal of this paper is to analyze the effect of recombination and ionization on the analysis of Mach and single probes in un-magnetized and magnetized plasmas. With a fast-scanning probe and Thomson scattering (TS) systems, global change of density and electron temperature with neutral pressure and effect on the deduction of Mach numbers are to be analyzed by new one-dimensional fluid models along with existing two-dimensional fluid model.

2. Experimental setup

MAP-II device [4] generates plasmas by an arc discharge between a flat LaB6 cathode disk (diameter 30 mm) and an anode pipe in the source region, which consists of a plasma source and a dual chamber connected by a drift tube improving gas isolation. A core plasma stream about 5 cm in diameter is transmitted along a longitudinal magnetic field of about 200 G. The density of the plasmas in the first chamber (source chamber) is relatively high ($3\times10^{13}\,\mathrm{cm}^{-3}$), while that in the second chamber (target chamber) is lower ($2\times10^{12}\,\mathrm{cm}^{-3}$). DiPS [5] is developed for analysis of electric probes with magnetic field effect, collision of charged particles and neutrals, probe shape and materials, and plasma and transport parameters, which is composed of three major parts: a divertor simulator with LaB6 DC plasma source (diameter = 100 mm, magnetic field up to 2 kG, $T_i \approx 0.2$–0.7 eV), a material processing simulator with helicon plasma source, and a space simulator without magnetic field. The typical electron temperature and density are 2–3 eV and up to $10^{14}\,\mathrm{cm}^{-3}$ for an Ar plasma and 5–10 eV and up to $10^{13}\,\mathrm{cm}^{-3}$ for a He plasma.

Various electric probes (single, emissive, Mach) are installed on the fast-scanning probe systems, whose typical speed is about 1 m/sec and components are pneumatic cylinder, solenoid valves, optical limit switches, and bellows sectors. Total length of the probe assembly is about 100 cm and its stroke is 30 cm. Fig. 1 shows the schematic views of a fast-scanning probe system and probe geometries in un-magnetized plasma MAP-II ($B = 200$ G, $\rho_i = 2.8(\mathrm{H}) \sim 5.5(\mathrm{He})$, $a_p = 1.4$ mm, $P_n = 5$–150 mTorr) and magnetized plasma at DiPS ($B = 1.1$ kG, $\rho_i = 1.31(\mathrm{He})$, $a_p = 3$ mm, $P_n = 0.8$–50 mTorr). A TS [6] system is installed on MAP-II having a lens with a focal length of 1 m focuses the beam in the center of the plasma through a Brewster window and three baffle plates. A second harmonic Nd:YAG Laser ($\leqslant$400–500 mJ/pulse @ 532 nm, 7 ns, 10 Hz) is used as the probe beam of the TS systems.

3. Models

To see the effect on recombination on the axial profile of density, one may use an analytic solution in cylindrical geometry after separating the radial and axial components with classical diffusion in low magnetic field as in the Q-machine [7], then one can obtain the following equation for axial variation of plasma density from steady-state continuity and momentum equation assuming quasi-neutrality:

$$n(z) \propto \exp[-m(Sn_c z)^2/4T], \tag{1}$$

where S, n_c, m, T are effective volume recombination rate ($\langle\sigma v\rangle_{\mathrm{rec}}$), plasma density at $z = 0$, ion mass and plasma temperature, respectively. Assuming the uniform plasma source profile, the overall ambipolar diffusion and radial classical diffusion, the radial density profile in the cylindrical plasma has the form of

$$\frac{n(s)^2}{n_0^2} \equiv N_1(s) = b + cI_0(s) \quad (0 \leqslant s \leqslant s_1),$$
$$N_2(s) = dI_0(s) + eK_0(s) \quad (s_1 \leqslant s \leqslant s_2), \tag{2}$$

where b, c, d, e are constants to be determined by the boundary conditions ($N_1(0) = 1$, $N_1(s_1) = N_2(s_1)$, $N_2(s_2) = 0$, $s_1 =$ source radius, $s_2 =$ wall radius), $s = r/R_0$, n_0 density at $r = 0$, and the relaxation length $R_0 = (\eta T/B_0^2 S)^{1/2}$. Here I_0, K_0, η, B_0 are the zeroth order modified Bessel functions of the

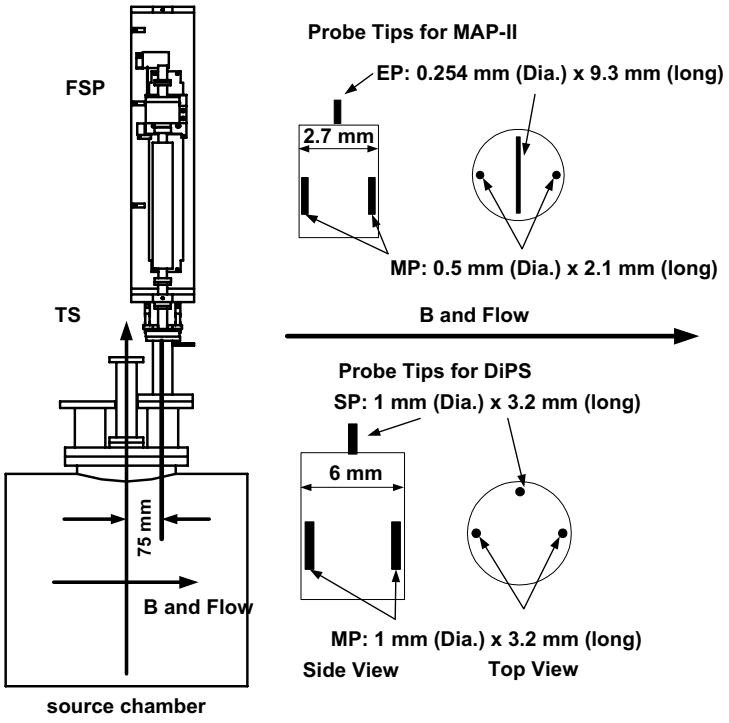

Fig. 1. Fast-scanning probe (FSP) system and probe geometries for MAP-II and DiPS experiments.

first and second kind, resistivity, external magnetic field, respectively, and the radial diffusion would be assumed to be classical to fit the radial profile in terms of recombination rate (S).

Using the Mach probe, composed of two opposite directional probes, the ratio (R) of ion saturation currents are measured in the upstream and downstream directions with strongly negative bias modes (e.g., $V_b = -150$ V), then the relevant Mach numbers (M), is deduced using appropriate theories of recombining and ionizing plasmas in the un-magnetized and magnetized plasmas. For this, consider a Boltzmann transport equation of ions

$$v\frac{\partial f}{\partial z}+\frac{q}{m}E_z\frac{\partial f}{\partial v}=S_t(v,z)+Gn_e(z)f_n(v)-Sn_e(z)f_i(z,v), \tag{3}$$

where $v \equiv v_z$, and the transport sources for the un-magnetized (I: $\rho_i > a$) and magnetized (II: $\rho_i < a$) cases are given as

$$S_t \approx \frac{v_i}{a}\left(1-\frac{n_i}{n_\infty}\right)f_\infty(\mathrm{I}),\quad \frac{D_\perp}{a^2}\left[\alpha(f_\infty-f_i)+(1-\alpha)\left(1-\frac{n_i}{n_\infty}\right)f_\infty\right](\mathrm{II}),$$

with $G=\langle\sigma v\rangle_{ion}$, $S=\langle\sigma v\rangle_{eir}+(1-\delta)\langle\sigma v\rangle_{dr}$, $\delta=[\langle\sigma v\rangle_{ic}n_i(H+)]/[\langle\sigma v\rangle_{dr}n_i(AH+)]$, and the subscripts ion, eir, dr, ic mean by ionization, electron–ion recombination, dissociative recombination, and ion conversion, respectively. Here $D_\perp$ is the anomalous cross-field diffusivity, $a = a_p$ is the probe radius (or size), and $\alpha(\equiv\eta_\perp/n_i m D_\perp)$ is the normalized shear viscosity. f_∞ is a shifted Maxwellian with ion temperature, T_i, and f_n is a Maxwellian with neutral temperature, T_n. For mono-atomic particles δ is almost unity excluding molecular activated recombination (mar $\approx$ ic + dr). With quasi-neutrality, $n_e = Zn_i$, and Boltzmann electrons, taking the zeroth and first moments lead to the following equations for both the un-magnetized ($\rho_i > a$) and magnetized plasmas ($\rho_i < a$), separately:

$$\frac{dn}{dM}=n\frac{[\tau(1-n)(M_\infty-2M)-2\sigma_1 nM+\rho_1 n^2 M]}{\tau(1-n)(1-M_\infty M+M^2)+\sigma_1 n(1+M^2)-\rho_1 n^2}, \tag{4}$$

$$\frac{dn}{dM}=n\frac{[M_\infty-nM-(1-\alpha)n(M_\infty-M)+2\sigma_2 nM-\rho_2 n^2 M]}{[1-n-M(M_\infty-M)[1-(1-\alpha)n]+\sigma_2 n(1-M^2)-\rho_2 n^2]}, \tag{5}$$

where the following dimensionless variables are used: $M \equiv V_z/C_s$, $M_\infty \equiv V_d/C_s$, $n \equiv n_i/n_\infty$, $y \equiv z/a$ (for $\rho_i > a$), z/L (for $\rho_i < a$), $L \equiv a^2 C_s/D_\perp$, $\tau \equiv v_i/$

$C_s = [T_i/(T_i+ZT_e)]^{0.5}$, $\sigma_1 = GZan_n/C_s$, $\sigma_2 = (GZan_n/C_s)(L/a)$, $\rho_1 = SZan_\infty/C_s$, $\rho_2 = (SZan_\infty/C_s)(L/a)$, and $C_s \equiv [(T_i + ZT_e)/m_i]^{0.5}$. Although these equations may produce values larger than $n = 1$ for $\alpha = 0$ [8,9], the sheath values ($n_s = n$ ($M = -1$)) for various M_∞ do not change for $\alpha \neq 0$ and non-zero values of $\rho_{1,2}$ and $\sigma_{1,2}$. This is shown by getting non-singular solutions of $n(y)$ and $M(y)$ including small ionization and charge-exchange in solving dn/dy and dM/dy, separately, and calculate the sheath values [10].

4. Result and analysis

Both MAP-II (un-magnetized) and DiPS (magnetized) plasmas are usually generated at pressure of several mTorr. Fig. 2 shows the variations of plasma density and electron temperature measured by a single probe comparing with those by TS. Both

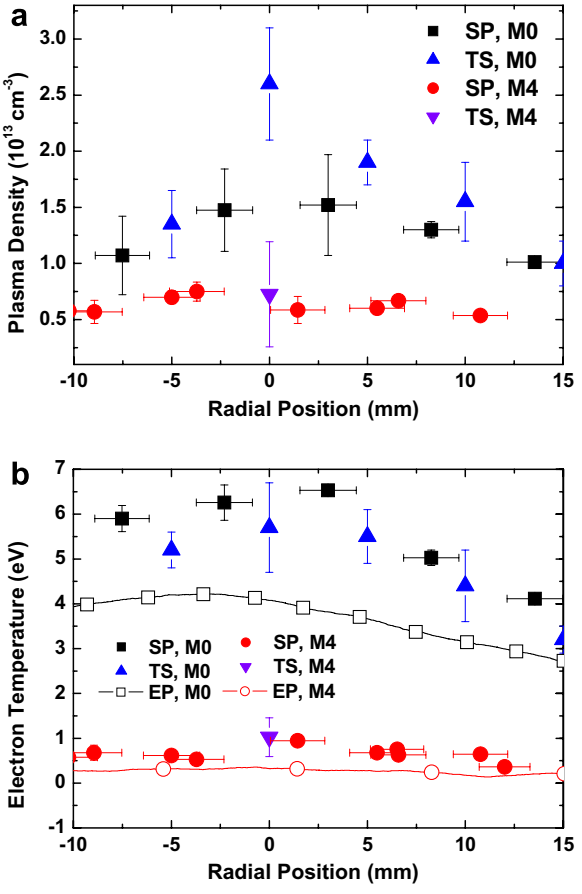

Fig. 2. Measurement of plasma density and electron temperature via single probe (SP), emissive probe (EP) and Thomson scattering (TS) at ionizing plasma ($P_n = 5.5$ mTorr). (a) Plasma density, (b) electron temperature. M0 = mode 0, M4 = mode 4.

electron temperature and plasma density measured by electric probe seem to agree well with those by TS within experimental error. Electron temperatures deduced from the floating and plasma potentials measured by an emissive probe are also added, and they are smaller than those by electric probe and TS methods.

From the MAP-II data, consider the ionizing case (mode 0) at the center ($Z = 1$ and $T_i \approx T_n = 0.1T_e$ are assumed): $B = 200$ G, $a = 1.35 \times 10^{-3}$ m, $P_n = 5.5$ mTorr, $T_e = 6$ eV, $n_\infty = 1.5 \times 10^{19} m^{-3}$, then the relevant numbers for helium become as $C_s = 1.199 \times 10^4$ m/sec, $\lambda_D = 4.699 \times 10^{-6}$ m, $\rho_i = 7.9 \times 10^{-3}$ m, $n_n \approx 7.63 \times 10^{18}$ m^{-3}, $\tau = 0.3$, $\sigma_1 = 2.2 \times 10^{-4}$, $\rho_1 = 1.7 \times 10^{-7}$. Then the recombining case (mode 4) at the center ($Z = 1$ and $T_i \approx T_n = 0.1$, T_e is assumed): $B = 200$ G, $a = 1.35 \times 10^{-3}$ m, $P_n = 112$ mTorr, $T_e = 1$ eV, $n_\infty = 7 \times 10^{18}$ m^{-3}, then the relevant numbers for helium become as $C_s = 4.895 \times 10^3$ m/sec, $\lambda_D = 2.808 \times 10^{-6}$ m, $\rho_i = 3.226 \times 10^{-3}$ m, $n_n \approx 9.32 \times 10^{19}$ m^{-3}, $\tau = 0.3$, $\sigma_1 = 6 \times 10^{-8}$, $\rho_1 = 2 \times 10^{-6}$.

In DiPS device, we obtain the data for the following pressure modes: $P_n = 0.8$ (mode 1), 4.8 (mode 2), 27 (mode 3), and 53 (mode 4) mTorr. For the reaction rates in DiPS, they are increased by a factor of L/a, which is ~10 for the following conditions: $B_0 = 1100$ G, $n_e = 3.5 \times 10^{12}$ cm^{-3}, $T_e = 8.5$ eV (mode 1), $n_e = 9 \times 10^{12}$ cm^{-3}, $T_e = 3$ eV (mode 4). Then the normalized transport) (τ), ionization (σ_2) and recombination (ρ_2) rates for modes (1, 4) are (0.3, 0.3), (7×10^{-3}, 2×10^{-3}) and (2×10^{-9}, 2×10^{-6}), respectively.

Since the contribution from ionization and volume recombination in both MAP-II (unmagnetized) and DiPS (magnetized) is too small ($\sigma_1 = 6 \times 10^{-6}$–$2.2 \times 10^{-4}$, $\rho_1 = 1.7 \times 10^{-7}$–$2 \times 10^{-6}$, $\sigma_2 = 7 \times 10^{-4}$–$2 \times 10^{-3}$, $\rho_2 = 2 \times 10^{-9}$–$2 \times 10^{-6}$), comparing with that from transport ($\tau = 0.3$), the relation between the flow velocity with the ion current density ratio is almost the same as that without these contribution of atomic processes, i.e., the maximum change in ratio (R) with drift velocity (M_∞) is about 0.4% for recombination case, and less than 2% for ionization case, which results less difference in the flow velocity in the logarithm form. So one can use analytic formulae of collisionless models for the un-magnetized (Eq. (4) with $\sigma_1 = 0 = \rho_1$) and magnetized cases (Eq. (5) with $\sigma_2 = 0 = \rho_2$ or [11]) such as $M_\infty = 2\ (R-1)/(R+1)$, ($\rho_i > a_p$), and $M_\infty = \ln(R/K)$, ($\rho_i < a_p$), where $K = (2+2\alpha)/(2+\alpha) + (\alpha \arctan(1+\alpha)^{0.5})/(1+\alpha)^{0.5}$.

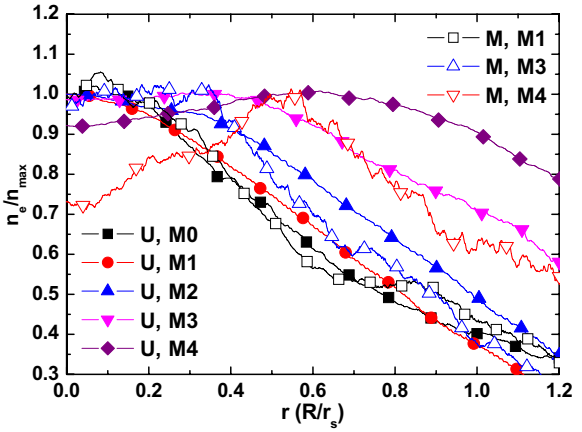

Fig. 3. Normalized radial density profile of MAP-II (Solid legends) and DiPS (Open legends). Plasma size (r_s (mm)) of MAP-II is 25 and for DiPS 15. First legends *M* means by magnetized and *U* by un-magnetized, the second *Mx* indicates mode *x*.

Fig. 3 shows the variations of normalized plasma densities of MAP-II and DiPS. The peak density varies as $1.8\times10^{13}\ \mathrm{cm}^{-3}\sim4\times10^{12}\ \mathrm{cm}^{-3}$ with pressure. Decay of central density may be fitted into Eq. (1) as $n_0/n_4=\exp[-(S_0^2/T_0-S_4^2/T_4)mn_c^2z_p^2/4]\approx4$, where z_p is the position where the fast-scanning probe is inserted (≈25 cm), 0 and 4 indicate the normal mode (mode 0) and mode 4. Here T_e, T_i, n_∞, n_n of two modes are given as (6, 1 eV), (0.6, 0.1 eV), (1.5×10^{13}, $7\times10^{12}\ \mathrm{cm}^{-3}$), ($7.7\times10^{12}\ \mathrm{cm}^{-3}$, $6.2\times10^{13}\ \mathrm{cm}^{-3}$). This is a fitting if n_c is assumed to be $\approx10^{16}$–$10^{17}\ \mathrm{cm}^{-3}$, which is the density at the surface of LaB6. From the normalized profiles, we can calculate the e-folding lengths (r_e) approximately as 23 (mode 0), 25 (mode 1), 30, 44, and 58 mm (mode 4), which are inversely dependent upon the relaxation length ($R_0=(\eta T/B_0^2\alpha)^{1/2}$) in Eq. (2). Since $\eta\propto T_e^{-3/2}$, $R_0\propto\alpha^{-1/2}T^{-1/4}$ for fixed B_0. Because R_0 is the relaxation length of $N(\equiv n^2/n_0^2)$, it would be better use $r_e(4)/r_e(0)=[R_0(0)/R_0(4)]^{0.5}$. From given experimental data, $r_e(4)/r_e(0)$ is 48/23 = 2.09 and $[R_0(0)/R_0(4)]^{0.5}$ is as 1.36, and there seems to be a large difference. However, if we take the humped profile of mode 4 into consideration, the ratio of r_e becomes 1.43, which is close to the inverse of relaxation length. Radial density profile becomes broader with neutral pressure, indicating that the recombination makes the profile broader, or ionization does the profile steeper, which is consistent with the simple planar diffusion model [12]. The humped profiles at higher pressures in both devices are yet to be explained.

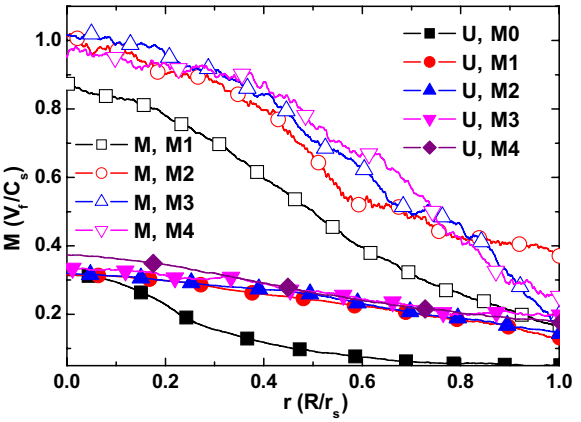

Fig. 4. Mach Numbers of MAP-II (Solid legends) and DiPS (Open legends).

Fig. 4 shows the variations of Mach numbers deduced by using approximation of Eqs. (4) and (5), and those by kinetic, fluid and PIC models for MAP-II ($\rho_i > a$) and DiPS ($\rho_i < a$) [11,13,14]. Mach numbers of central region at 25 cm from the LaB6 source in MAP-II are about 0.3–0.4, which are 7% larger than those by Hutchinson's and 20% smaller than those by Eq. (4), while those in DiPS is close to unity, which are taken at about 110 cm from the LaB6 source. The latter might be due to steep pressure gradient and magnetic expansion near the end of open chamber. For the DiPS date, we use the average calibration factor of Chung (or Eq. (5)) and Hutchinson for the magnetized plasmas, i.e., $K=(2.02+2.33)/2=2.18$ [11].

5. Conclusion

The overall change of density profile has been explained by a two-dimensional fluid model with uniform source in terms of volume recombination. To deduce the flow velocity from the Mach probe measurement, we introduced a new one-dimensional fluid model including ionization and recombination in addition to the transport source which reflects the two-dimensional effect both in the un-magnetized and magnetized flowing plasmas.

Recombination with neutral pressure affects the overall change of plasma density (n_∞) and electron temperature (T_e), yet it does not give large impact on the deduction of the local Mach numbers ($M(r)$) due to small values of both reaction rates. However, the absolute magnitude of flow velocity decreases with recombination (or neutral pressure) due to reduction of electron temperature. If neutral

pressure is very high as in the private regions or larger connection length of the flux tube (L) of existing and future toroidal divertor machines, contribution from recombination would become larger due to strong magnetic field ($L/a \gg 1$) and neutral pressure (strong i–n collision) comparing linear machines, then it will affect the deduction of the Mach numbers, which is often calculated as supersonic, yet it might be subsonic in reality.

Acknowledgements

This work is done during the visit of the first author to the High Temperature Plasma Center of the University of Tokyo, which is greatly appreciated. This work is supported by the National Research Laboratory (NRL) Project of the Korea Science and Engineering Foundation (KOSEF) under the Korea Ministry of Science and Technology (MOST).

References

[1] P.C. Stangeby, The Plasma Boundary of Magnetic Fusion Devices, Institute of Physics Publishing, Bristol, 2000.
[2] S.I. Krasheninnikov, A.Yu. Pigarov, D.J. Sigmar, Phys. Lett. A 214 (1996) 285.
[3] R.K. Janev, T. Kato, J.G. Wang, Phys. Plasmas 7 (2000) 4364.
[4] S. Kado, H. Kobayashi, T. Oishi, S. Tanaka, J. Nucl. Mater. 313–316 (2003) 754.
[5] K.-S. Chung et al., Contribution Plasma Phys. 46 (2006) 364.
[6] S. Kado et al., J. Plasma Fusion Res. 81 (2005) 810.
[7] K.-S. Chung, S.H. Hong, J. Appl. Phys. 53 (1882) 6702.
[8] I.H. Hutchinson, Phys. Plasmas 2 (1995) 1794.
[9] K.-S. Chung, Phys. Plasmas 2 (1995) 1796.
[10] K.-S. Chung, Y.-S. Choi, M.-J. Lee, H.-J. Woo, 32nd EPS Conference on Controlled Fusion and Plasma Physics, Tarragona, Spain (2005) P2.079.
[11] K.-S. Chung, Phys. Plasmas 1 (1994) 2864.
[12] M.A. Liebermann, A.J. Lichtenberg, Principles of Plasma Discharges and Material Processing, John Wiley, New York, 1994, Chapter 5.
[13] K.-S. Chung, J. Appl. Phys. 69 (1991) 3451.
[14] I.H. Hutchinson, Plasma Phys. Control. Fus. 44 (2002) 1953.